Magnetic response of a two-dimensional viscous electron fluid

AYDIN CEM KESER

OLEG SUSHKOV

Magnetic response of a two-dimensional viscous electron fluid

Aydın C. KESER[1,2,*], **Oleg P. SUSHKOV**[1,2]
[1]School of Physics, University of New South Wales, Sydney, Australia
[2]Australian Research Council Centre of Excellence in Future Low-Energy Electronics Technologies,
University of New South Wales, Sydney, Australia

Abstract: It has been established that the Coulomb interactions can transform the electron gas into a viscous fluid. This fluid is realized in a number of platforms, including graphene and two-dimensional semiconductor heterostructures. The defining characteristic of the electron fluid is the formation of layers of charge carriers that are in local thermodynamic equilibrium, as in classical fluids. In the presence of nonuniformities, whirlpools and nontrivial flow profiles are formed, which have been directly imaged in recent experiments. In this paper, we theoretically study the response of the electron fluid to localized magnetic fields. We find that the electric current is suppressed by viscous vortices in regions where magnetic field is sharply varying, causing strong transport signatures. Experimentally, our considerations are relevant since local magnetic fields can be applied to the system through implanting adatoms or embedding micromagnets in the top-gate. Our theory is essential for the characterization and future applications of electron fluids in hydrodynamic spin transport.

Keywords: Carrier dynamics, dissipative dynamics, electrical conductivity, friction, interparticle interactions, magnetotransport

1. Introduction

The hydrodynamic transport of electrons has been the subject of intense research in recent years [1–4]. Electron transport is usually dominated by impurity scattering in ordinary conductors, where the electrons behave like a diffusive gas. In sufficiently pure samples, Coulomb interactions transform the electron system into a viscous fluid [3–6]. The early prediction of an 'electron fluid' in solids, made by Gurzhi [7, 8] has been confirmed experimentally with the discovery of high purity samples [9].

Notable consequences of fluid behavior that has been demonstrated by recent studies are: the decrease of resistance with increasing temperature (Gurzhi effect)[2, 9–11], Poiseuille flow profiles [12–15], negative nonlocal resistance and formation of whirlpools [16, 17], Hall viscosity [18, 19], negative magnetoresistance [2, 20, 21], the violation of the Wiedemann-Franz law [22–26], anomalous scaling of resistance with channel width [23, 27], and quantum-critical dynamic conductivity [28]. Moreover, many novel phenomena have been proposed, such as hydrodynamic spin transport [29, 30] inspired by experiments on liquid mercury [31, 32].

The defining characteristic of hydrodynamic transport is the formation of layers of charge carriers

---

*Correspondence: a.keser@unsw.edu.au

that are in local thermodynamic equilibrium, as in classical fluids [39]. In uniform flow, the layers are at rest with respect to a common inertial frame. On the other hand, in the presence of nonuniformities, whirlpools and non-trivial flow profiles are formed. These flow patterns can be directly imaged, as in recent sophisticated experiments [12–15].

In this paper, we focus on the magnetic response of the two-dimensional (2D) electron fluid. Our motivation is two-fold. Firstly, magnetic response of classical fluids is a curious phenomenon called 'Moses effect' [40] with applications in colloidal chemistry. Akin to this effect, we find that the electron fluid streamlines deform to avoid regions where magnetic fields vary sharply.

Secondly, the magnetic manipulation of the 2D electron fluid is now a practical reality in a number of platforms such as Co adatoms on graphene [33–36], or micromagnets embedded in the top gate of a semiconductor heterostructures [37, 38]. Moreover, magnetic response of the electron fluid is essential for its characterization and future technological applications, such as hydrodynamic spin transport [32].

In an ultrapure system, when the temperature is comparable to the Fermi energy, electrons scatter much more often with each other, than they do with phonons and impurities [1, 2]. As a result, local thermodynamic equilibrium is established within a region of size comparable to the electron-electron (e-e) scattering length. Above this length scale, electrons can be described like a classical fluid that obeys the Navier-Stokes equation [4, 39]. In the presence of an out-of-plane magnetic field, the Lorentz force affects the electron fluid. A uniform magnetic field cannot deflect the electron flow owing to the incompressibility of electron fluid, and merely creates a Hall pressure (voltage), whereas nonuniform fields can have a nontrivial effect on the flow profile.

The main findings of our paper are: (i) that the nonuniform localized magnetic field creates vorticity in the system, (ii) a magnetic impurity of size comparable to the e-e scattering length induces Lorentz force gradients so strongly that, current flow is suppressed near the impurity and electron flow is expelled out of this vicinity, and finally (iii) the viscous energy loss due to magnetically induced vortices cause large resistive contributions to transport.

The plan of the paper is as follows. In Seciton 2 we write down the fluid equations of motion that describes the system. We show that under realistic experimental conditions, the equations of motion become linear in current density, and there is a natural length scale in the system arising from the interaction of electrons with each other and also with phonons and impurities. This length scale separates the viscous dominated (ultraviolet) and drag dominated (infrared) regions. In Section 3 we consider the 'magnetic Stokes problem', where a uniform flow is incident on a region that contains out-of-plane magnetic field. In Section 4 we perturbatively determine the flow profile of electrons, when both the magnetic field and its gradients are weak. In Section 5, we show that the perturbative theory breaks down near a magnetic impurity, and a logarithmic renormalization of current density takes effect. In Section 6 we calculate the transport signature of localized magnetic fields on the system. Finally, Section 7 is devoted to the conclusions.

2. The magnetohydrodynamics of the electron fluid

In this section we describe the physical model of the 2D electron flow under simultaneous application of electrochemical potential gradients and out-of-plane magnetic field, in terms of the modified incompressible Navier-Stokes equation

$$\mathbf{v}/\tau + \mathbf{v} \cdot \nabla \mathbf{v} - \nu \nabla^2 \mathbf{v} = -\nabla \Phi / m^* - |e|/m^* \mathbf{v} \times \mathbf{B}. \tag{2.1}$$
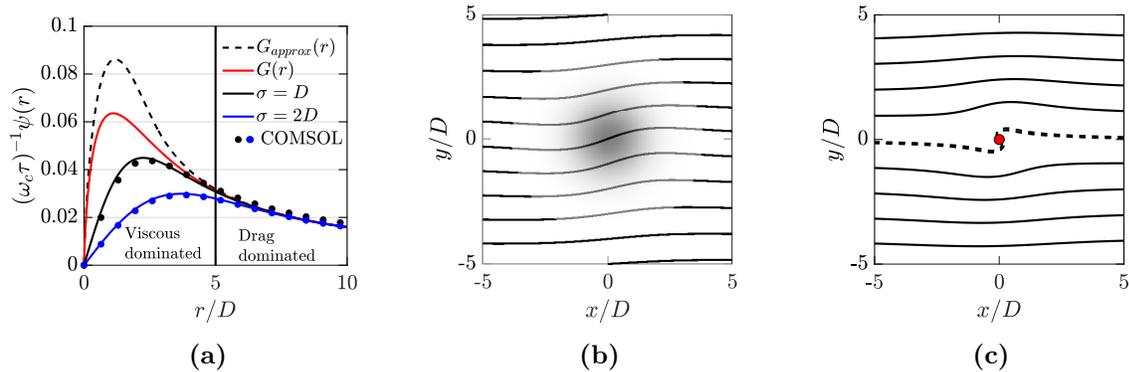
Figure 1. The electrons follow curves of constant streamfunction Ψ, called the streamlines. In the Stokes problem, we assume a uniform flow of electrons in the x-direction is incident on a localized magnetic field region. a) The radial part of the normalized correction to the stream function in the weak field intensity and soft gradient regime. The total streamfunction is $\Psi = -v_0 y + v_0 D \psi(r) \cos(\varphi)$. The out-of-plane magnetic field $\mathbf{B} = \hat{\mathbf{z}} B b(r)$ is assumed to be radially symmetric with a Gaussian profile $b(r, \sigma)$ centered around the origin with a standard deviation σ. The solid blue and black curves are the analytic solutions (see Equation (4.12)) for, $\sigma = D, 2D$, respectively. The filled circles are data points obtained by simulating the system on COMSOL Multiphysics software [42] with weak field parameters. Notice that the blue circles have a closer agreement with theory, since the analytic solution is obtained in the weak gradient limit. In the limit $\sigma \to 0$, the profile becomes a delta function, hence we recover the radial part of the Green's function in Equation (4.11), shown by solid red curve. The flow is viscous dominated close to the origin and drag dominated further away. The transition occurs around $r = 5D$. The Green's function can be piecewise constructed in these asymptotic regions, respectively, as $G_<, G_>$ in Equation (4.9), shown by the dashed black curve b) The streamlines of an electric current incident on a magnetic field region with soft Gaussian profile. The current in the x-direction is deflected by the out-of-plane magnetic field concentrated in the dark region. c) A magnetic impurity creates a sharply changing magnetic field profile and induces large Lorentz force gradients. Hence, the perturbative solution no longer holds. Instead, the current near the impurity is logarithmically suppressed, therefore the streamline passing through the origin (dashed lined) does not carry current. Here, the small radius of the impurity $r_0 = 0.2D$ serves as the ultraviolet (UV) logarithmic cut-off. In (b) and (c) the magnetic field is exaggerated to make the streamline deformation more prominently visible.

Here $\mathbf{v}$ is the electron fluid velocity vector field that is incompressible $\nabla \cdot \mathbf{v} = 0$. The velocity field is related to the electric current density and electron number density as $\mathbf{J} = -|e|n\mathbf{v}$. The collision time τ is responsible for momentum loss scattering processes such as those due to phonons and impurities, and creates an effective drag on the fluid. The kinematic viscosity ν is the intrinsic property of the electron fluid calculated from its interaction Hamiltonian. In 2D $\nu = v_F l_{ee}/4$ holds, where v_F is the Fermi velocity and l_{ee} is the e-e scattering length. Φ is the electrochemical potential, m^* is the effective mass of the electron. Finally, $\mathbf{B}$ is the out of plane magnetic field. Based on real experiments, for example [2], we consider low currents $\sim 200 \, \text{nA}$. with typical velocities about $200 \, \text{m/s}$, in a system with length $10 \, \mu\text{m}$. Meanwhile, the kinematic viscosity is very large, $\nu \sim 200 \, \text{cm}^2/\text{s}$ making the electron fluid nearly 300 times thicker than honey. As a result, the Reynolds number turns out to

be Re ~ 0.01. This means then nonlinear Navier term, $\mathbf{v} \cdot \nabla \mathbf{v}$, responsible for inertial forces due to convective acceleration, is a hundred times smaller than viscous forces. Therefore, we neglect this term and work with the linear Stokes equation. The realistic range of parameters are given in Table 1.

It is known that the viscosity of electron fluid depends on the applied magnetic field [41], and additional Hall viscous friction emerges [19]. However, both of these effects are second order in the B-field and therefore negligible, since the deviation due to B-field is $\delta\nu/\nu \sim 1\%$.

We can parametrize the Stokes equation as

$$\mathbf{v} - D^2\nabla^2\mathbf{v} = -\tau\nabla\Phi/m^* - \omega_c\tau b(\mathbf{x})\mathbf{v} \times \hat{\mathbf{z}}, \qquad (2.2)$$

where $D = \sqrt{\nu\tau}$ is the momentum diffusion length, which can also be expressed in terms of the geometric average $D = \sqrt{l_{ee}l_{mfp}}/2$ of two length scales. These are, namely, the e-e scattering length l_{ee} that conserves momentum in the electron system and mean free path of collisions of electrons with impurities and phonons, that subtracts momentum from the electron system. The product $\omega_c = |e|B/m^*$ is the cyclotron frequency and b captures the spatial dependence of the magnetic field. We define the stream function as

$$v_y = \partial_x\Psi, \quad v_x = -\partial_y\Psi,$$
$$v_r = -\frac{1}{r}\partial_\varphi\Psi, \quad v_\varphi = \partial_r\Psi, \qquad (2.3)$$

so that the incompressibility constraint $\nabla \cdot \mathbf{v} = 0$ is automatically satisfied. The curves with constant Ψ values are called streamlines. The velocity field is, by definition, everywhere tangent to the curves of equal Ψ, that is, the particles follow the streamlines.

3. The magnetic stokes problem

We imagine the realistic scenario where a uniform flow of electrons in the x-direction is incident on a magnetic field distribution centered around the origin. The stream function can be decomposed into a part that generates the uniform flow and a correction term due to the magnetic field induced vorticity:

$$\Psi = -v_0y + v_0D\psi, \quad \omega = \hat{z} \cdot \nabla \times \mathbf{v} = v_0D\nabla^2\psi. \qquad (3.1)$$

Now taking the curl of the Stokes equation Equation (2.2) we obtain

$$\nabla^2\Psi - D^2\nabla^4\Psi = \omega_c\tau\nabla b(\mathbf{x}) \cdot \mathbf{v}. \qquad (3.2)$$

We note that, when the magnetic field is uniform, the right-hand side vanishes and therefore the streamlines are trivial, $\Psi = -v_0y$. The incoming flow is not affected but a classical Hall voltage, $V_y = -m^*\omega_cv_0W$, develops in the system with width W.

To find the response to a nonuniform field, it is beneficial to find the Green's function that solves the above equation for $b = \delta(x)$ up to normalization constants. Below, we construct the Green's function in weak and strong magnetic fields.

4. Perturbative solution in weak magnetic field with a soft gradient

When the magnetic field strength and the gradient is weak, the source term in Equation (3.2), $\omega_c \tau \nabla b \cdot \mathbf{v} \ll v_0/D$. Therefore, the corrections to the incoming velocity v_0 is small. We therefore apply first order perturbation theory and take the velocity in the source term on the right-hand side of Equation (3.2) to zeroth order. We can work in the normalized units where

$$v_0 = D = 1. \tag{4.1}$$

Then the Green's function obeys

$$\nabla^2 G - \nabla^4 G = \partial_x \delta(\mathbf{x}). \tag{4.2}$$

Before solving this problem exactly, we use scaling analysis to have an intuitive grasp of the problem. In the regions $r > R \sim 1$ and $r < R \sim 1$, the dominant operators are ∇^2 and ∇^4, respectively. In the large r regime we may write

$$\nabla^2 G_> = \partial_x \delta(\mathbf{x}). \tag{4.3}$$

We can recognize this from electrostatics and solve it as

$$G_> = G(r \to \infty) \to \frac{1}{2\pi} \partial_x \log(r) = \frac{\cos(\varphi)}{2\pi r}. \tag{4.4}$$

Meanwhile for $r < R \lesssim 1$ we have

$$-\nabla^2 \omega_< = \partial_x \delta(\mathbf{x}). \tag{4.5}$$

Needless to say this has the same solution; however, we can add a function harmonic in the unit circle to the solution:

$$\omega_< = -\frac{\cos(\varphi)}{2\pi r} + \frac{R^{-2}}{2\pi} r \cos(\varphi). \tag{4.6}$$

This choice is judicious so that $\omega_<(R) = \omega_>(R) = 0$ at the matching point. Now solving for the stream function in polar coordinates, we obtain

$$\partial_r(r^{-1}\partial_r(rG_<)) = \left(-\frac{1}{2\pi r} + \frac{R^{-2}}{2\pi} r\right) \cos(\varphi), \tag{4.7}$$

which implies

$$G_< = G(r \to 0) \to \frac{\cos(\varphi)}{4\pi} \left(-r \log(r) + Ar + R^{-2}\frac{r^3}{4}\right). \tag{4.8}$$

Note that this solution diverges to infinity if $r \sim R \to \infty$. This infrared (IR) divergence is essentially the Stokes paradox where the creeping flow solution does not exist in 2D [39]. IR divergence is automatically cured in our problem because momentum loss terms define a finite length scale $D = \sqrt{\nu \tau} \equiv 1$, and therefore, the $G_<$ is only valid in the bounded region $r < R \sim 1$.

At the boundary of viscous to ohmic flow, $r = R$, we demand G and $\partial_r G$ to be continuous. From these constraints we obtain

$$G(r \gg R = 2\sqrt{2}) \to \frac{\cos(\varphi)}{2\pi r}, \tag{4.9a}$$

$$G(r \ll R = 2\sqrt{2}) \to \left(\frac{r^3}{64} - \frac{r}{4}\log\left(\frac{r^2}{8}\right)\right)\frac{\cos(\varphi)}{2\pi}, \tag{4.9b}$$

the radial part of which is plotted in Figure 1a as dashed lines. The exact Green's function defined as the solution of Equation 4.2 can be obtained in momentum space as

$$G(k) = -\frac{ik_x}{k^2(1+k^2)}.$$

(4.10)

In real space this is

$$G = \frac{\cos(\varphi)}{2\pi} \int_0^\infty dk \frac{J_1(kr)}{1+k^2} = \frac{\cos(\varphi)}{2\pi r}[1 - rK_1(r)],$$

(4.11)

where K_1 is the modified Bessel function of the second kind of order 1. Therefore, asymptotic behavior of G matches Equation (4.9). The radial part of the exact Green's function is shown in Figure 1a.

Now we can write down the solution for a weak an arbitrary distribution $b(\mathbf{x})$ with soft gradients

$$\psi(\mathbf{k}) = -\omega_c\tau \frac{ik_x b(\mathbf{k})}{k^2(1+k^2)},$$

(4.12)

where $\psi = \Psi + y$ is the correction to the stream function in real space, and $\psi(\mathbf{k})$ is its Fourier pair. For a radially symmetric and Gaussian magnetic field distribution $b(r, \sigma)$ with standard deviation σ, we can plot the radial part of the normalized correction to the stream function in Figure 1a for $\sigma = D, 2D$. As expected, when $\sigma \to 0$, the Gaussian profile approaches a delta function hence we recover the exact Green's function Equation (4.11), up to normalizing constants.

As seen in Figure 1b, the electron trajectories are bent due to Lorentz force gradients. As a measure of this, we can calculate the transverse velocity $v_y(0)$ at the center of the magnetic domain, with a gaussian profile, as

$$v_y(0) = \partial_x\psi = \frac{\omega_c\tau}{8\pi} \int_0^\infty d\alpha \frac{e^{-\alpha/2}}{\sigma^2 + \alpha} = \frac{\omega_c\tau}{8\pi} e^{\sigma^2/2} \mathrm{E}_1(\sigma^2/2), \quad \text{(perturbative)}.$$

(4.13)

Here $\mathrm{E}_1(z) = \int_z^\infty dt \exp(-t)/t$ is the exponential integral. When the standard deviation is large, the Lorentz Force gradients are weak and the transverse velocity decays as $v_y(0) \sim v_0\omega_c\tau D^2/(4\pi\sigma^2)$. In the limit of strong gradients, $\sigma \to 0$, we have $v_y(0) \sim \log(D/\sigma)$ and the perturbation theory breaks down as expected.

5. Logarithmic suppression of velocity near a magnetic impurity in the strong field, strong gradient limit

A magnetic impurity with size $r_0 \ll D$ creates a large magnetic field gradient, that is, the source term in Equation (3.2) becomes large $\omega_c\tau\nabla b \cdot \mathbf{v} \gg v_0/D$. Therefore, the conditions for a perturbative reduction of the magnetic Stokes problem Equation (3.2) to Equation (4.2) are not fulfilled.

Once again, we work in the normalized units where

$$D = v_0 = 1,$$

(5.1)

unless otherwise stated, and reintroduce D or v_0, wherever convenient. We restore physical units in the plots and in calculating the estimates. Modelling the magnetic impurity as a delta function, we solve Equation (3.2) as

$$\psi(\mathbf{k}) = -\omega_c\tau \frac{i\mathbf{k} \cdot \mathbf{v}(r \to 0)}{k^2(1+k^2)},$$
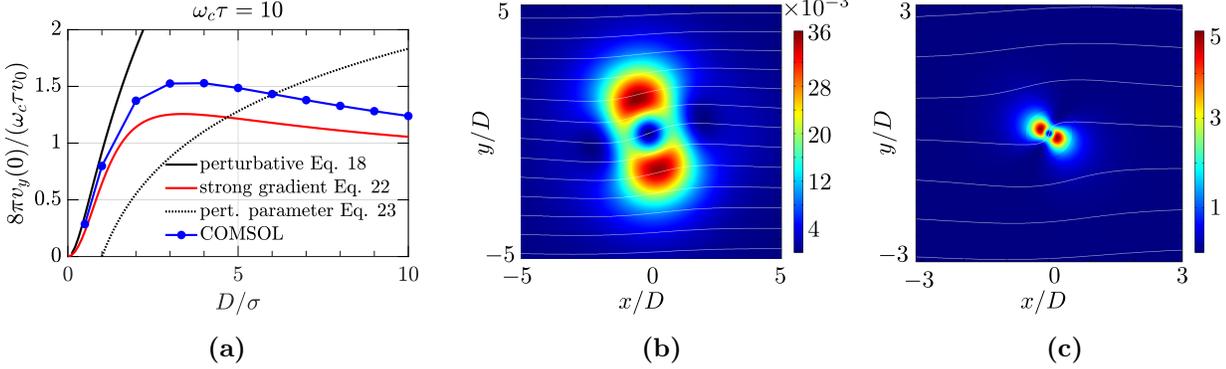
(5.2)

Figure 2. a) Normalized transverse velocity at the center of magnetic region, fixed as origin, plotted against the sharpness of the Gaussian magnetic field distribution with standard deviation σ. A strong magnetic field $\omega_c\tau = 10$ is chosen to highlight the transition from perturbative to strong gradient regimes. The solid black line shows the soft gradient perturbation theory result, which agrees with the numerical solution, as also indicated in Figure 1a. The dotted black line is the perturbation theory parameter A in Equation (5.5). The perturbation theory breaks down when the parameter $A \approx 0.5$. The solid red curve is from the strong gradient solution Equation (5.4), which shows the logarithmic suppression at the origin. The COMSOL Multiphysics [42] simulations, shown by the blue dots, agree with the strong gradient calculation up to logarithmic accuracy. b-c) Distribution of viscous power density in real space, normalized to the uniform ohmic dissipation $(nev_0)^2\rho_\tau \approx 0.05\,\mathrm{W/m^2}$. The simulation is performed on COMSOL. The white curves are the streamlines. The magnetic field is chosen to be large ($\omega_c\tau = 10$) for better visibility of streamline deformation. The viscous dissipation is due to a Gaussian magnetic field distribution with standard deviation σ. The perturbative limit with soft gradient $\sigma = D$ is shown in (b) and the strong field, strong gradient $\sigma = D/10$ is realized in (c). Note that the power dissipation is suppressed at the origin, which is a consequence of the Gaussian magnetic field distribution.

where $\psi = \Psi + y$ and $\psi(\mathbf{k})$ is its Fourier pair. For self-consistency, we require the velocity near the origin to satisfy the relations in Equation (2.3):

$$v_x(0) = 1 + \omega_c\tau \int \frac{d^2k}{(2\pi)^2} ik_y \frac{ik_x v_x(0) + ik_y v_y(0)}{k^2(1 + k^2)}, \tag{5.3a}$$

$$v_y(0) = -\omega_c\tau \int \frac{d^2k}{(2\pi)^2} ik_x \frac{ik_x v_x(0) + ik_y v_y(0)}{k^2(1 + k^2)}. \tag{5.3b}$$

Solving these we have

$$v_x(0) \to \frac{1}{1 + A^2}, \quad v_y(0) \to \frac{A}{1 + A^2}, \tag{5.4}$$

where, after restoring D,

$$A = \frac{\omega_c\tau}{8\pi} \log\left(1 + D^2/r_0^2\right) \to \frac{\omega_c\tau}{4\pi} \log(D/r_0), \tag{5.5}$$

and $r_0 \ll D$ is the ultraviolet cut-off scale. This scale is determined by the physical size of the impurity and the e-e interaction length l_{ee}. Below $r < l_{ee} \sim 200\,\mathrm{nm}$, hydrodynamic theory progressively

breaks down as the electrons can not locally equilibrate to form the fluid. Therefore, realistically, the logarithm can not grow more than $\log(D/l_{ee}) \sim 1$. This means that a transition from perturbation theory to strong field regime should occur for large $\omega\tau$ leading to $A \lesssim 1$. Figure 2a shows that the transition from soft to strong gradient regimes, and the logarithmic suppression occurs around $A \approx 0.5$, that is equivalent to $\omega_c\tau \approx 6$ or $B \approx 90\,\text{mT}$ according to Table 1. The numerical simulations agree with the strong field theory up to logarithmic accuracy.

We can find ψ of Equation (5.2) in real space, by using the result in Equation (4.11). When $r \ll D$ we have

$$\Psi = -y + \frac{\omega_c\tau}{4\pi}(v_x(0)x + v_y(0)y)\log(D/r). \tag{5.6}$$

We note that, the 0th streamline that passes close to the origin $r \sim r_0$ (with value $\psi \sim 1/\log^2(D/r_0)$) does not carry any velocity since,

$$v_x|_{y \to r_0} = -\partial_y\psi|_{y \to r_0} \to 0, \tag{5.7}$$

meaning that the fluid avoids the singularity by deforming around it. The streamlines are shown in Figure 1c. This situation is a similar to the Moses effect, where a diamagnetic fluid evacuates regions of magnetic field [40]. Here, the Lorentz force gradient on the charge fluid becomes very large near the impurity and expels the flow lines outwards.

Table 1. Parameters of electron system at $30\text{-}40\,\text{K}$, based on the experiment in Keser et al. [2].

Parameter	Expression	Value	Description
m^*	$0.067m_e$	$6.1 \times 10^{-32}\,\text{kg}$	Effective electron mass
n		$2.45 \times 10^{11}\,\text{cm}^{-2}$	Electron density
E_F	$\hbar^2\pi n/m^*$	$8.8\,\text{meV},\ 100\,\text{K}$	Fermi energy
l_{ee}		$200\,\text{nm}$	e-e interaction length scale
l_{mfp}	$v_F\tau_{mfp}$	$5.9\,\mu\text{m}$	Mean free path
D	$\sqrt{l_{ee}l_{mfp}}/2$	$0.54\,\mu\text{m}$	Momentum diffusion length
τ_{mfp}		$27.7\,\text{ps}$	Momentum relaxation time
ρ_τ	$(ne^2\tau/m^*)^{-1}$	$35\,\Omega$	Ohmic resistivity
μ	$e\tau_{mfp}/m^*$	0.7 million $\text{cm}^2/(\text{Vs})$	electron mobility
B^*	$m^*v_F/(2el_{ee})$	$204.2\,\text{mT}$	Characteristic viscous magnetic field
$\varphi_c^* = \omega_c^*\tau$	$eB^*\tau/m^*$	14.9	Cyclotron parameter at characteristic field

6. Viscous dissipation and resistance

The deformation of streamlines as shown in Figure 1 results in viscous stresses. From the Stokes Equation (2.2), we can find the rate of energy dissipation due to the viscous forces as the integral of the viscous power density (that is the work done against the viscous force per unit time):

$$\dot{E}_\nu = -\nu m^* n \int d^2x\, \mathbf{v} \cdot \nabla^2\mathbf{v}, \tag{6.1}$$

where n is the number density of electrons. Figures 2b and 2c show the distribution of viscous power dissipation in real space for weak and strong gradient limits. By using the definition Equation (2.3) of the stream function, and using Fourier methods we can write the dissipation in physical units, in terms of a dimensionless integral

$$\dot{E}_\nu = \nu m^* n v_0^2 D^2 \int \frac{d^2 k}{(2\pi)^2} k^4 |\psi(\mathbf{k})|^2. \tag{6.2}$$

Since $\dot{E}_\nu = R_\nu I^2$, we can find the induced viscous resistance in a system with an effective width W, for which the current is $I = W|e|nv$. We express the viscous resistance in terms of the Drude resistance $\rho_\tau = m^*/(ne^2\tau)$ as

$$R_\nu/\rho_\tau = \frac{D^2}{W^2}(\omega_c\tau)^2 f(D/r_0), \tag{6.3}$$

for some dimensionless form factor f that depends on the characteristic length scale of the magnetic field distribution r_0.

In a system with length L and width W that contains magnetic impurities with number density n_m, the contribution to resistivity $\rho_{\nu,m} = R_\nu W/L$ is

$$\rho_{\nu,m} = \rho_\tau D^2 n_m (\omega_c\tau)^2 f. \tag{6.4}$$

For a radially symmetric soft magnetic field distribution $b(r,\sigma)$ considered in Section 4, this form factor is

$$f(s = \sigma/D) = \int_0^\infty \frac{d\alpha}{8\pi} \frac{\alpha e^{-s^2\alpha}}{(1+\alpha)^2} = \frac{-1 + (1+s^2)e^{s^2}\mathrm{E}_1(s^2)}{8\pi}, \quad \text{(perturbative)}, \tag{6.5}$$

where E_1 is the exponential integral. The exponential suppression of the integrand in k space is reflected in Figures 2b and 2c as suppression of power density at the origin. When $\sigma \gtrsim D$, the denominator of the integrand is $(1+\alpha)^2 \sim 1$, within the relevant range of integration. Therefore, for soft magnetic field profile, the function f decays rapidly as $f \sim D^4(8\pi\sigma^4)^{-1}$. The hydrodynamic theory becomes less accurate at scales smaller than the e-e interaction length l_{ee}, at which thermodynamic equilibration is established. For this reason, we shall take $r_0 \sim l_{ee}$ and therefore $f \approx 1/(8\pi)$.

In the delta function limit $\sigma/D \to r_0/D \ll 1$, the term $e^{-s^2\alpha} \to 1$, in the numerator of the integrand, hence we have a logarithmic divergence within the perturbative approach:

$$f \to \frac{1}{4\pi} \log D/r_0, \quad \text{(perturbative)}. \tag{6.6}$$

However, this is cured by the fact that, near a delta function, there is a further logarithmic suppression of velocity, as discussed in Section 5. All in all, the resistance due to a sharp magnetic field distribution, for which $\omega_c\tau \log(D/r_0) \gtrsim 1$, is renormalized as

$$f \to \frac{4\pi \log(D/r_0)}{(4\pi)^2 + (\omega_c\tau)^2 \log^2(D/r_0)}, \quad \text{(renormalized)}. \tag{6.7}$$

Once again, we shall take $r_0 \sim l_{ee}$ and therefore $\log(D/r_0) \sim 1$. Working with logarithmic accuracy, we have essentially the same result as in Equation (6.5). In order to have viscous resistivity

to be comparable to the Drude resistivity, arising from nonmagnetic impurities, we need, based on the Table 1,

$$n_m \approx \frac{1}{4\pi D^2}\left(1 + \left(\frac{4\pi}{\omega_c \tau}\right)^2\right) \sim 10^9 \, \text{cm}^{-2}, \quad @B \approx 20\,\text{mT}, \tag{6.8}$$

corresponding to about 10 micromagnetic impurities per micron squared. To compare, the electron number density is about a 200 times larger than this value. Realistically, if we increase the field to $B \approx 90\,\text{mT}$, we can achieve a 100% correction to resistivity $\rho_{\nu,m} = \rho_\tau$ for 1 micromagnet per micron squared.

7. Conclusion

In this paper, we considered the response of the two-dimensional viscous electron fluid to a localized out-of-plane magnetic field. From a purely theoretical perspective, this problem is akin to the Stokes problem for a 2D classical fluid. A drag force acts on the electron fluid arising from the scattering of electrons from the impurities and phonons in the system. The drag force acts on the long wavelength limit and cures the infrared divergence of the Stokes paradox. The drag and viscous forces define a natural length scale, the momentum diffusion length D, in the system. We find that, when the magnetic field in concentrated in a region small compared to D, as in the case of a magnetic impurity, solutions perturbative in the field and gradient strength break down in the ultraviolet region. This is saved by the logarithmic renormalization of fluid velocity near the impurity. Physically, this is because the large Lorentz force gradients near the impurity expels electric current. We demonstrate that this logarithmic suppression is crucial in predicting the experimental consequences of having micromagnets or magnetic adatom impurities in the system. We show that this effect introduces a large contribution to the resistivity of the system. Our findings are applicable to a wide range of platforms, including graphene and ultrapure semiconductor heterostructures.

Acknowledgements

References

[1] B. Narozhny, "Hydrodynamic approach to two-dimensional electron systems," *La Rivista del Nuovo Cimento* **45** (2022) 661.

[2] A. C. Keser, D. Q. Wang, O. Klochan, D. Y. H. Ho and O. A. Tkachenko et al., "Geometric Control of Universal Hydrodynamic Flow in a Two-Dimensional Electron Fluid," *Physical Reiew X* **11** (2021) 031030.

[3] M. Pollini and A. Geim, "Viscous electron fluids," *Physics Today* **73** (2020) 28.

[4] A. Lucas and K. C. Fong "Hydrodynamics of electrons in graphene," *Journal of Physics: Condensed Matter* **30** (2018) 053001.

[5] B. N. Narozhny, I. V. Gornyi, A. D. Mirlin and J. Schmalian, "Hydrodynamic Approach to Electronic Transport in Graphene," *Annalen Der Physik* **529** (2017) 1700043.

[6] J. Zaanen, "Electrons go with the flow in exotic material systems," *Science* **351** (2016) 1026.

[7] R. N. Gurzhi, "Hydrodynamic Effects in Solids at Low Temperature," *Soviet Physics Uspekhi* **11** (1968) 255.

[8] R. N. Gurzhi, "Minimum of Resistance in Impurity- Free Conductors," *J .Exptl. Theoret. Phys.* **44** (1963) 771.

[9] M. J, M. de Jong and L. W. Molenkamp, "Hydrodynamic electron flow in high-mobility wires," *Physical Review B* **51** (1995) 13389-13402.

[10] R. Krishna Kumar, D. A. Bandurin, F. M. D. Pellegrino, Y. Cao, and A. Principi, et al., "Superballistic flow of viscous electron fluid through graphene constrictions," *Nature Physics* **13** (2017) 1182.

[11] L. V. Ginzburg, C. Gold, M. P. Röösli, C. Reichl and M. Berl et al., "Superballistic electron flow through a point contact in a Ga[Al]As heterostructure," *Physical Review Research* **3** (2021) 023033.

[12] J. A. Sulpizio, L. Ella, A. Rozen, J. Birkbeck and D. J. Perello et al., "Visualizing Poiseuille flow of hydrodynamic electrons," *Nature* **576** (2019) 75.

[13] M. K. H. Ku, T. X. Zhou, Q. Li, Y. J. Shin and J. K. Shi et al., "Imaging viscous flow of the Dirac fluid in graphene," *Nature* **583** (2020) 537.

[14] B. A. Braem, F. M. D. Pellegrino, A. Principi, M. Röösli, and C. Gold et al., "Scanning gate microscopy in a viscous electron fluid," *Physical Review B* **98** (2018) 241304.

[15] L. Ella, A. Rozen, J. Birkbeck, M. Ben-Shalom and D. Perello et al., "Simultaneous voltage and current density imaging of flowing electrons in two dimensions," *Nature Nanotechnology* **14** (2019) 480.

[16] A. O. Govorov, and J. J. Heremans, "Hydrodynamic Effects in Interacting Fermi Electron Jets," *Physical Review Letters* **92** (2004) 026803.

[17] D. A. Bandurin, I. Torre, R. K. Kumar, M. Ben Shalom and A. Tomadin et al., "Negative local resistance caused by viscous electron backflow in graphene," *Science* **351** (2016) 1055.

[18] G. M. Gusev, A. D. Levin, E. V. Levinson and A. K. Bakarov, "Viscous transport and Hall viscosity in a two-dimensional electron system," *Physical Review B* **98** (2018) 161303.

[19] A. I. Berdyugin, S. G. Xu, F. M. D. Pellegrino, R. Krishna Kumar, A. Principi et al., "Measuring Hall viscosity of graphene's electron fluid," *Science* **364** (2019) 162.

[20] Q. Shi, P. D. Martin, Q. A. Ebner, M. A. Zudov and L. N. Pfeiffer et al., "Colossal negative magnetoresistance in a two-dimensional electron gas," *Physical Review B* **89** (2019) 201301.

[21] R. G. Mani, A. Kriisa and W. Wegscheider, "Size-dependent giant-magnetoresistance in millimeter scale GaAs/AlGaAs 2D electron devices," *Scientific Reports* **3** (2013) 2747.

[22] J. Crossno, J. K. Shi, K. Wang, X. Liu and A. Harzheim et al., "Observation of the Dirac fluid and the breakdown of the Wiedemann-Franz law in graphene," *Science* **351** (2016) 1058.

[23] J. Gooth, F. Menges, N. Kumar, V. Süss and C. Shekhar et al., "Thermal and electrical signatures of a hydrodynamic electron fluid in tungsten diphosphide," *Nature Communications* **9** (2018) 4093.

[24] A. Jaoui, B. Fauqué, K. Behnia, "Thermal resistivity and hydrodynamics of the degenerate electron fluid in antimony," *Nature Communications* **12** (2021) 195.

[25] A. Lucas and S. Das Sarma, "Electronic hydrodynamics and the breakdown of the Wiedemann-Franz and Mott laws in interacting metals," *Phys. Rev. B* **97** (2018) 245128.

[26] S. Ahn and S. Das Sarma, "Hydrodynamics, viscous electron fluid, and Wiedeman-Franz law in two-dimensional semiconductors," *Physical Review B* **106** (2022) L081303.

[27] P. J. W. Moll, P. Kushwaha, N. Nandi, B. Schmidt and A. P. Mackenzie, "Evidence for hydrodynamic electron flow in $PdCoO_2$," *Science* **351** (2016) 1061.

[28] P. Gallagher, C. Yang, T. Lyu, F. Tian and R. Kou, "Quantum-critical conductivity of the Dirac fluid in graphene," *Science* **364** (2019) 158.

[29] G. Tatara, "Hydrodynamic theory of vorticity-induced spin transport," *Physical Review B* **104** (2021) 184414.

[30] R. J. Doornenbal, M. Polini and R. A. Duine, "Spin–vorticity coupling in viscous electron fluids," *Journal of Physics: Materials* **2** (2019) 015006.

[31] R. Takahashi, M. Matsuo, M. Ono, K. Harii and H. Chudo et al., "Spin hydrodynamic generation," *Nature Physics* **12** (2016) 52.

[32] R. Takahashi, H. Chudo, M. Matsuo, K. Harii and Y. Ohnuma et al., "Giant spin hydrodynamic generation in laminar flow," *Nature Communications* **11** (2020) 3009.

[33] J. Ren, H. Guo, J. Pan, Y. Y. Zhang and X. Wu et al., "Kondo Effect of Cobalt Adatoms on a Graphene Monolayer Controlled by Substrate-Induced Ripples," *Nano Letters* **14** (2014) 4011.

[34] B. Uchoa, V. N. Kotov, N. M. R. Peres and A. H. Castro Neto, "Localized Magnetic States in Graphene," *Physical Review Letters* **101** (2008) 026805.

[35] T. O. Wehling, A. V. Balatsky, M. I. Katsnelson, A. I. Lichtenstein and A. Rosch, "Orbitally controlled Kondo effect of Co adatoms on graphene," *Physical Review B* **81** (2010) 115427.

[36] V. W. Brar, R. Decker, H. Solowan, Y. Wang and L. Maserati et al., "Gate-controlled ionization and screening of cobalt adatoms on a graphene surface," *Nature Physics* **7** (2011) 43.

[37] R. Neumann, L. R. Schreiber, "Simulation of micro-magnet stray-field dynamics for spin qubit manipulation," *Journal of Applied Physics* **117** (2015) 193903.

[38] J. N. Engdahl, A. C. Keser, and O. P. Sushkov, "Micromagnets dramatically enhance effects of viscous hydrodynamic flow in a two-dimensional electron fluid," *Physical Review Research* **4** (2022) 043175.

[39] L. D. Landau, E. M. Lifshitz, "Fluid Mechanics," Elsevier Science (2013) .

[40] E. Bormashenko, "Moses effect: physics and applications," *Advances in Colloid and Interface Science* **269** (2019) 1.

[41] P. S. Alekseev, "Negative Magnetoresistance in Viscous Flow of Two-Dimensional Electrons," *Physical Review Letters* **117** (2016) 166601.

[42] COMSOL Multiphysics® v. 5.1, COMSOL AB, Stockholm, Sweden (2015).